EPJ Web of Conferences **301**, 02005 (2024) https://doi.org/10.1051/epjconf/202430102005
XLV Symposium on Nuclear Physics 2024

Effect on incomplete fusion of breakup fragments of the weakly bound projectile ^{8}B in reactions with targets ^{27}Al, ^{28}Si, ^{208}Pb and ^{209}Bi

A. Gomez Camacho[1,*]

[1]Departamento de Aceleradores y Estudio de Materiales, Instituto Nacional de Investigaciones Nucleares, Apartado Postal 18-1027, C.P. 11801, México, D.F.

Abstract.
Calculations of total, complete and incomplete fusion cross sections are presented as function of the incident energy of the weakly bound projectile ^{8}B in reactions with light ^{27}Al, ^{28}Si and heavy ^{208}Pb and ^{209}Bi mass targets. In particular, the relative effect of the breakup fragments; proton and ^{7}Be of ^{8}B on incomplete fusion is determined. Also, the effect of an additional proton to the nuclear potential of the targets ^{28}Si, ^{209}Bi respect to ^{27}Al and ^{208}Pb is determined as a function of the incident energy. It is found that the proton absorption becomes more important than for ^{7}*Be* for light targets for energies around and above the barrier, however, the inverse occurs for heavy targets. The calculations are performed with two different methods. The CDCC to determine the relative projectile-target radial wave functions which subsequently are used in the angular momentum-dependent model of fusion probabilities to calculate complete, incomplete and total fusion.

1 Introduction

Recently, nuclear mechanisms of fusion and breakup reactions induced by weakly bound projectiles have been intensely studied both theoretically and experimentally [1–6]. The most investigated weakly bound nuclei are ^{6,7}Li, ^{9}Be, ^{8}B, and unstable ^{6,8}He, ^{7,11}Be and ^{17}F in reactions with a variety of stable targets. In fact, the effect of breakup of weakly bound projectiles on other mechanisms such as elastic scattering and fusion have been the focus of strong attention, since these effects can be very pronounced. Even though, reactions with exotic beams are presently available, most of the experimental research centers on measurements with stable weakly bound nuclei. This is so, since the intensities of these beams are several orders of magnitude larger than those for exotic beams. Most experiments determine fusion and elastic scattering cross sections because direct measurements of breakup yields are difficult to carry out. However, by using coincidence techniques, exclusive breakup yields have been measured for the system ^{6}Li+^{59}Co [7, 8], not only for elastic but also for sequential breakup from several transfer/pick up mechanisms. It is well known that reactions with weakly bound projectiles give rise to very specific fusion reaction processes. For instance, complete fusion (CF) which occurs when the whole projectile is captured by the target. CF can be direct (DCF) when fusion takes place without a previous breakup, or it can be sequential (SCF),

*e-mail: arturo.gomez@inin.gob.mx

when all projectile fragments are captured after breakup. Incomplete fusion (ICF) is another mechanism in which, after breakup, only some fragments are captured by the target while others fly away to the continuum. Total fusion (TF) is the sum of CF and ICF. Moreover, non-capture breakup (NCBU) is the process in which, none of the fragments is captured by the target. NCBU can be elastic, in which case, the fragments interact elastically with the target. Otherwise can be inelastic, *i.e.,* when inelastic excitations of the target and/or projectile (prior to breakup) are produced. All of these breakup processes, including pickup and transfer are schematically represented in Ref. [9] for the weakly bound ^{6,7}Li. As a matter of fact, a realistic evaluation of the effect of breakup on fusion must take into account couplings to all of the collective degrees of freedom involved in the reaction. Several studies that consider the effect of projectile breakup on complete fusion have been published in recent years [7–11]. Basically, it is found that CF becomes suppressed at energies around and below the Coulomb barrier. This suppression has been mainly associated to the low threshold energy of the weakly bound projectile, that results in a loss of flux of intact incident nuclei at the Coulomb barrier. At sub-barrier energies, the study of the reaction mechanisms produced by this type of nuclei may be more complex. For instance, sequential breakup produced after nucleon transfer or pickup are processes that may predominate over direct breakup, that enhance SCF [12–15]. For example, for the two-body nuclei ^{6}Li ($\alpha - d$) and ^{7}Li ($\alpha - t$), recent measurements [12] have established that significant breakup of ^{6}Li is triggered by neutron transfer that leads to sequential $p - \alpha$ breakup of the projectile-like nucleus ^{5}Li. Or d-pickup by ^{6}Li, leading to sequential breakup of $^8\text{Be} \rightarrow \alpha + \alpha$. For ^{7}Li, important breakup intensities have been observed for p-pickup that produces $\alpha + \alpha$ coincidences, and $2n$-stripping, that leads to sequential $p + \alpha$ breakup. On the other hand, direct breakup of ^{6,7}Li also has an important effect on fusion at low energies, mainly by its contribution to ICF. That is, since ICF becomes increasingly relevant for decreasing incident energies, therefore, the direct breakup process inhibits CF.

Theoretical studies that take into account all of the above mentioned reaction processes become extremely complicated. For that reason, to reduce the complexity only the most significant reaction channels (elastic, some inelastic and direct breakup) are commonly taken into consideration. Among the most used theoretical approaches is the CDCC method [10, 11, 16–18]. This model is applied to quantify the effect of continuum breakup states on several reaction observables particularly on fusion. In this model, reaction projectiles with core-valence cluster structure, like ^{6}Li, ^{7}Li or ^{8}B, fusion is calculated with the use two short-range absorption potentials W_{F_1} and W_{F_2} to account for capture of each fragment F_2, F_2 [19, 20]. In principle, CF (both direct and sequential) can be obtained when both fragments are inside the absorption region of these potentials. ICF when only one fragment is captured by its respective absorption potential, while the other flies away to the continuum and survives the capture process. Now, the incomplete fusion of a given fragment, say, F_1, is determined by imposing $W_{F_2} = 0$ and vice versa. Using this technique, Parkar et al., [20] calculated fusion cross sections for reactions of ^{6,7}Li with targets ^{209}Bi and ^{198}Pt. However, although, their calculations of CF and ICF have a good agreement with the experimental data, there is a shortcoming in their approach. In the sense that, the contributions to ICF of the fragments of the projectile are performed by separate calculations. That is, the calculations are not self-consistent since the cross sections for each fusion process are done by a different CDCC calculation. Another theoretical approach to determine CF and the contributions to ICF from the fragments, is the three dimensional classical dynamical model [21, 22]. This model permits explicit calculation of sequential and direct CF, as well as, the contribution to ICF from the projectile fragments [23]. In this approach, breakup is treated stochastically and its probability is assessed from either breakup observables or CDCC calculations. In this model, the breakup probability of the projectile as a function of its distance to the target has a fundamental effect on the de-

termination of CF and ICF at energies near the barrier. The Classical Dynamical model has been used with success in different reactions at energies close and above the Coulomb barrier but not at energies below.

In the present work, a study of fusion excitation functions of the very weakly bound projectile ^{8}B ($E_{thre} = -0.137$ MeV) with targets of light, ^{27}Al, ^{28}Si and heavy ^{208}Pb, ^{209}Bi masses is presented. Calculations of total, complete and incomplete fusion cross sections are determined by the recently proposed angular momentum-dependent model of fusion probabilities [24–26]. Particular emphasis is given to the effect on incomplete fusion of increasing mass and charge of the target. On the same footing, the effect on the contributions to ICF from the fragments proton and ^{7}Be is investigated as a function of the incident projectile energy. Another interesting calculation here shown, concerns how fusion is affected by an additional proton to the nuclear potential of the target. These type calculations are presented for the nuclei ^{27}Al respect to ^{28}Si and, ^{208}Pb respect to ^{209}Bi. The basic details of the theoretical model are given in section II, while the calculations and discussion of the results, are presented in section III. Finally, in section IV, a summary and conclusions are given.

2 Basic details of CDCC and angular momentum fusion probabilities

Calculations of fusion cross sections are performed with the CF-ICF computer code [27] that determines fusion in terms of angular momentum expansion of fusion probabilities of,

$$\sigma_{TF} = \frac{1}{\kappa^2}\frac{k}{E} < \Psi^{(+)}|\hat{W}|\Psi^{(+)} > . \tag{1}$$

A detailed description of this methology is given in Refs. [24–26]. In Eq. (1), κ is a normalization constant of the scattering wave function, k the incident wave number, E the incident energy while the total wave function $\Psi^{(+)}$ given by,

$$\Psi^{(+)}(\mathbf{R},\mathbf{r}) = \sum_{n=0}^{N} \psi_n(\mathbf{R}) \otimes \phi_n(\mathbf{r}), \tag{2}$$

here, $\psi_n(\mathbf{R})$ is the relative projectile-target radial wave function, $\phi_n(\mathbf{r})$ are the internal wave functions of the projectile, where $n = 0$ for the elastic incident channel and $n = 1...N$ for excited breakup states. Notice that only the ground state of the target is considered. The wave function $\Psi^{(+)}(\mathbf{R},\mathbf{r})$ is solution of the Hamiltonian,

$$\hat{H}(\mathbf{R},\mathbf{r}) = \hat{h}(\mathbf{r}) + \hat{T} + \hat{U}_1(\mathbf{r}_1) + \hat{U}_2(\mathbf{r}_2), \tag{3}$$

where, $\hat{h}(\mathbf{r})$ is the internal hamiltonian of the weakly bound projectile, $\hat{T}$ the relative kinetic energy in the center of mass of the system, while $\hat{U}_1(\mathbf{r}_1)$ and $\hat{U}_2(\mathbf{r}_2)$ are the interaction potentials between fragments F_1 and F_2 with the target. $\mathbf{r}_i,\ i = 1, 2$ represents the radial distance between the centers of mass of the target and the fragment F_i. Moreover, the interaction potentials between the fragments and the target are,

$$\hat{U}_i(\mathbf{r}_i) = \hat{V}_i(\mathbf{r}_i) - i\hat{W}_i(\mathbf{r}_i),\ i = 1, 2, \tag{4}$$

where, $\hat{V}_i(\mathbf{r}_i)$ includes the nuclear and Coulomb interactions between the fragment F_i and the target. $\hat{W}_i(\mathbf{r}_i)$ represents the corresponding absorption potential. The total absorption potential of Eq. (1) is,

$$\hat{W}(\mathbf{r}_1,\mathbf{r}_2) = \hat{W}_1(\mathbf{r}_1) + \hat{W}_2(\mathbf{r}_2). \tag{5}$$

For the calculations of total, complete and incomplete fusion cross sections in terms of angular dependent fusion probabilities [24–26], use will be made of the radial relative wave functions $\psi_n(R)$ of Eq.(2). These functions can be obtained from CDCC calculations. That is, the coupled-channel equations resulting from Eqs.(2) and (3) for the $n+1$ states. These equations are solved for a discrete breakup energy space that includes bound (B) and continuum states (C) of the projectile. These equations are given by,

$$\left[\hat{T}(R) + U_{\beta,\beta}(R) - (E - \varepsilon_\beta - \varepsilon_T)\right]\psi_\beta(R) = -\sum_{\beta'} U_{\beta,\beta'}(R)\psi_{\beta'}(R), \tag{6}$$

where the coupling matrices are,

$$U_{\beta\beta'}(R) = < \phi_\beta \left|\hat{V}_1(\mathbf{r}_1) + \hat{V}_2(\mathbf{r}_2)\right| \phi_{\beta'} >, \tag{7}$$

here, ε_β is the excitation energy of the projectile in the β-state, ε_T the ground state energy of the target and $U_{\beta,\beta}$, $U_{\beta,\beta'}$ are the radial dependent diagonal and non-diagonal coupling matrices of the interaction potentials between the ground and N continuum breakup states $\beta,\beta' = 0....N$. In fact, $\phi_\beta(r)$ are the square-integrable wave functions known as bin states. Iterative solutions of the coupled-channel equations are implemented in the code FRESCO [28], which we shall use in our calculations of the radial relative motion of the projectile-target wave function $\psi_\beta(R), \beta = 0....N$.

Total fusion cross section for a reaction of a weakly bound projectile composed of a two particle cluster structure can be written as,

$$\sigma_{TF} = \sigma_{DCF} + \sigma_{SCF} + \sigma_{ICF_1} + \sigma_{ICF_2}, \tag{8}$$

where σ_{DCF} is the direct complete fusion and σ_{SCF} the sequential complete fusion. Therefore, the complete fusion (CF) is given by,

$$\sigma_{CF} = \sigma_{DCF} + \sigma_{SCF}. \tag{9}$$

On the other hand, when only one fragment is captured by the target, while the other flies to the continuum, defines the incomplete fusion of that fragment σ_{ICF_i} $i = 1, 2$. Thus the incomplete fusion is $\sigma_{ICF} = \sigma_{ICF_1} + \sigma_{ICF_2}$. Now, if the total wave function $\Psi^{(+)}(\mathbf{R}, \mathbf{r})$ of Eq.(1) is split into bound (B) and continuum (C) sub-spaces of the projectile, *i.e.,*

$$\Psi^{(+)}(\mathbf{R}, \mathbf{r}) = \Psi^{(B)}(\mathbf{R}, \mathbf{r}) + \Psi^{(C)}(\mathbf{R}, \mathbf{r}), \tag{10}$$

where,

$$\Psi^{(B)}(\mathbf{R}, \mathbf{r}) = \sum_\alpha \psi_\alpha(\mathbf{R}) \otimes \phi_\alpha(\mathbf{r}), \tag{11}$$

and,

$$\Psi^{(C)}(\mathbf{R}, \mathbf{r}) = \sum_\gamma \psi_\gamma(\mathbf{R}) \otimes \phi_\gamma(\mathbf{r}), \tag{12}$$

in which, ψ_α, ψ_γ are the projectile-target relative radial wave functions for the bound (α) and continuum (γ) states. ϕ_α, ϕ_γ are the corresponding bound and breakup states of the projectile. Now, if matrix elements of the imaginary potentials of Eqs.(1) among bound states (B) to continuum states (C) of the projectile are negligible [19, 29, 30], then the following relations hold,

$$\sigma_{TF} = \sigma^B_{TF} + \sigma^C_{TF}, \tag{13}$$

where for bound states of the projectile,

$$\sigma^B_{TF} = \sigma^B_{DCF}, \tag{14}$$

and for breakup states,

$$\sigma_{TF}^{C} = \sigma_{ICF_1} + \sigma_{ICF_2} + \sigma_{SCF}. \tag{15}$$

In terms of fusion probabilities,

$$\sigma_{TF} = \frac{\pi}{k^2} \sum_J \sum_i (2J+1)\mathcal{P}_i^{(J)}, \tag{16}$$

where, J is the total angular momentum of the reaction and $i = DCF, ICF_1, ICF_2, SCF$. The first term is related to bound states (B) while the last three to continuum breakup states (C), *i.e.*,

$$\mathcal{P}_B^{(J)} = \mathcal{P}_{DCF}^{(J)}, \quad \mathcal{P}_C^{(J)} = \mathcal{P}_{ICF_1}^{(J)} + \mathcal{P}_{ICF_2}^{(J)} + \mathcal{P}_{SCF}^{(J)}. \tag{17}$$

These fusion probabilities can be calculated in terms of the so called projected angular momentum scattering wave function, which is obtained from Eq.(2), by projecting the intrinsic angular momentum wave function $\phi_n(\mathbf{r})$ of the projectile with angular momentum $\mathbf{j}_0$ onto the projectile-target relative radial wave function $\psi_n(\mathbf{R})$ with orbital angular momentum $\mathbf{L}_0$. See details in Appendix of Ref. [25]. Explicitly,

$$\sigma_{DCF}^{(B)} = \frac{\pi}{k^2} \sum_J (2J+1)\mathcal{P}_B^{(J)}, \tag{18}$$

is the direct complete fusion cross section obtained from bound (B) states of the projectile, also,

$$\sigma_{ICF_i} = \frac{\pi}{k^2} \sum_J (2J+1)\mathcal{P}_{ICF_i}^{(J)}, \quad i = 1, 2, \tag{19}$$

is the incomplete fusion of the fragments and,

$$\sigma_{SCF} = \frac{\pi}{k^2} \sum_J (2J+1)\mathcal{P}_{SCF}^{(J)}, \tag{20}$$

the sequential complete fusion.

To end this section, it should be emphasized that the above mentioned fusion probabilities satisfy the completeness relation,

$$\mathcal{P}_{el}^{(J)} + \mathcal{P}_{inel}^{(J)} + \mathcal{P}_{EBU}^{(J)} + \mathcal{P}_{TF}^{(J)} = 1. \tag{21}$$

The probabilities $\mathcal{P}_{el}^{(J)}$, $\mathcal{P}_{inel}^{(J)}$ and $\mathcal{P}_{EBU}^{(J)}$, are directly obtained from the CDCC calculations: Thus, it remains to determine $\mathcal{P}_{TF}^{(J)}$ and its components of Eq. (8), by the angular momentum projected version of fusion probabilities.

3 CDCC and Fusion Calculations

In the present work, we discuss comparative calculations of total, complete and incomplete fusion of reactions of the weakly bound nucleus ^{8}B with breakup threshold energy $E_{thre} = -0.137$ MeV, with targets ^{27}Al, ^{28}Si, ^{208}Pb and ^{209}Bi. As a first step, CDCC calculations of the radial projectile-target relative motion wave function $\psi_n(R)$ are performed, which in turn, are used to determine fusion probabilities for a given capture process. Capture of a breakup fragment of $^8B \rightarrow^7 Be + proton$, are calculated by using short range absorption potentials,

$$W_i = \frac{W_0}{1 + exp[(r_i - R_i/a_0]}, \tag{22}$$

where $i = 1, 2$, r_i is the distance between the fragment F_i to the center of mass of the target (T) and $R_i = r_0(A_i^{1/3} + A_T^{1/3})$, A_i being the mass of the fragment F_i. The parameters of $W_1(r)$ and $W_2(r)$ should be chosen such that, these potentials are well inside the potential barriers of the fragments and the target. Complete and incomplete fusion processes are included once, both or either fragment in their trajectories to the target, are/is inside the region of the absorption potentials. In the calculations here presented, the potential strength, the reduced radius and diffuseness parameters are fixed to $W_0 = 50$ MeV, $r_0 = 1.0$ fm, $a_0 = 0.2$ fm for both potentials $W_1(r)$ and $W_2(r)$ and for all targets. The real interactions $\hat{V}_i(\mathbf{r}_i)$ of Eq.(4) include the nuclear and Coulomb components. The nuclear potential is of SPP type [31, 32] while the radius of the Coulomb potential is set to $r_C = 1.3$ fm. On the othe hand, the nuclear interaction potential among the fragments $^7Be - p$ that produce a bound state of ^{8}B with binding energy $E_{thre} = -0.137$ MeV is that used in Ref. [33]. For incident energies above the Coulomb barrier, the discretized breakup energy space used in the CDCC calculations for ^{8}B is that of Ref. [33]. For energies below the barrier, some adjustments to this breakup discretized space are necessary to avoid numerical divergences, basically, this is done by reducing the upper limit of the excitation energy ϵ_{max} of the discrete breakup space.

In Figs. (1a-1d), the calculations of total, complete and incomplete fusion cross sections versus the incident energy E_{lab} are presented for reactions of ^{8}B with targets ^{27}Al, ^{28}Si, ^{208}Pb and ^{209}Bi. It is important to point out, that the fusion calculations here presented are systematic and that the same imaginary potential parameters are used for all reacting systems. Thus, it is expected that the calculations may not precisely agree with existing fusion data. A one by one calculation to fit the data particularly for the ^{28}Si target [34]. would require slight modifications to the potential parameters. These calculations are obtained from Eqs. (18-20), where $\sigma_{ICF} = \sigma_{ICF_1} + \sigma_{ICF_2}$ and $\sigma_{CF} = \sigma_{DCF} + \sigma_{SCF}$. It is observed that, for the lighter targets ^{27}Al, ^{28}Si, ICF is very important at low energies, close and below the barrier. In fact, as the energy decreases, ICF becomes the basic contributor to fusion, consequently the CF process becomes suppressed. This is due to the small value of the threshold energy of ^{8}B so that, few projectile bound nuclei remain intact as the incident beam approaches the target. For the heavy ^{208}Pb and ^{209}Bi, as seen in Figs. (1c) and (1d), CF accounts for most of the fusion process in the energy region around and above the barrier. For energies well below the barrier, it could be expected that ICF overcomes CF, however, these calculations result computationally complicated. Now, an interesting point to study is the effect on fusion of an additional proton in the upper shells of the target. That is the case of ^{28}Si respect to ^{27}Al and ^{209}Bi to ^{208}Pb. The additional proton slightly increases the Coulomb barrier and decreases its width, but on the other hand, the Coulomb repulsion is a bit stronger. However, the combined effect of these factors produces a smaller barrier height for ^{27}Al and ^{208}Pb respect to ^{28}Si and ^{209}Bi respectively. Hence, it is expected that at energies close to the barrier, the effect of the additional proton of ^{28}Si and ^{209}Bi, slightly suppresses fusion. This effect is observed in Figs. (1a), (1b) and (1c) and (1d), not only for total fusion but for complete and incomplete fusion. An estimate of the additional proton of ^{28}Si and ^{209}Bi on incomplete fusion, can be seen in Figs. (2a) and (2b), where the ratio $R = \sigma_{ICF}/\sigma_{TF}$ is presented. The first thing to notice is that R is larger for lower mass targets than for the heavier. For the nuclei ^{27}Al and ^{28}Si, as the energy decreases towards the barrier, ICF becomes enhanced while CF suppressed, then, $R = \sigma_{ICF}/(\sigma_{CF} + \sigma_{ICF})$ assumes values approaching unity. Also, it is observed that, the suppression of CF is somewhat larger for ^{28}Si than for ^{27}Al, therefore, R takes slightly higher values for ^{28}Si. For larger energies, the importance of the additional proton of ^{28}Si becomes negligible. As for the nuclei ^{208}Pb and ^{209}Bi a different behavior appears. For these nuclei, CF is the most significant fusion process at all energies, so that, CF accounts for most of TF. Thus, R assumes smaller values than for the lighter nuclei. As the energy increases above the barrier, ICF reactions start to grow at a higher rate than CF, so does R. However, as the

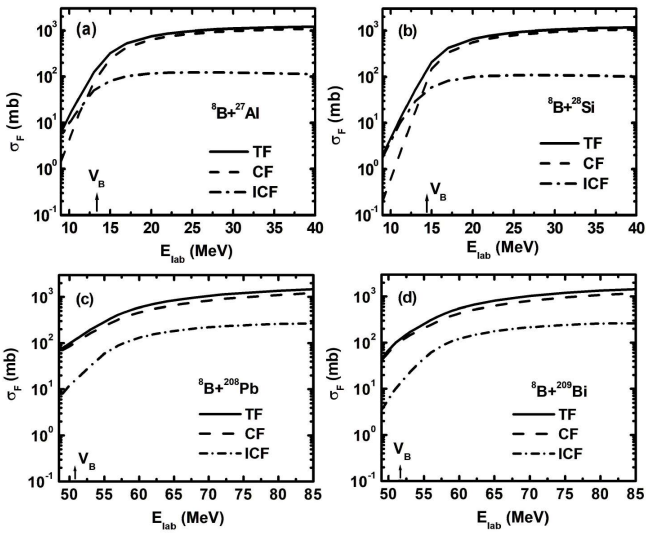

Figure 1. Total, Complete and Incomplete fusion cross sections for ^{8}B with the indicated targets.

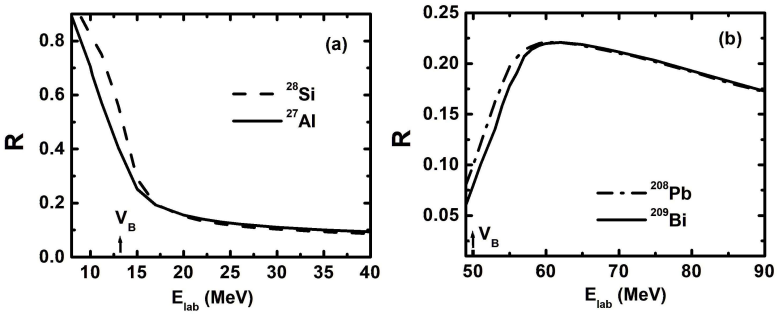

Figure 2. Ratio of incomplete fusion to total fusion for ^{8}B with the different targets.

energy becomes even larger, ICF processes stabilize, but σ_{CF} keeps rising, therefore R starts to take lower values. It is interesting to calculate the behavior of R at even lower energies, well below the barrier, however computational divergences emerge. Another key point to investigate is the specific role of incomplete fusion of the proton (σ_{ICF_p}) and of ^{7}Be ($\sigma_{ICF_{^7Be}}$) to the total incomplete fusion σ_{ICF} as functions of the incident energy E_{lab}. The incomplete fusion of the fragments p and ^{7}Be can be determined from Eq. (19). The results of these calculations are shown in Figs. (3a-3d) for the targets ^{27}Al, ^{28}Si, ^{208}Pb and ^{209}Bi respectively. It is observed, that the effect of incomplete fusion of the proton is more significant than that of ^{7}Be for the lighter nuclei ^{27}Al and ^{28}Si. On the other hand, for the more massive targets ^{208}Pb and ^{209}Bi, as shown in Fig. (3c-3d), $\sigma_{ICF_{^7Be}}$ overcomes σ_{ICF_p}. It is then observed, that the target mass is a key factor to determine the relative contributions to incomplete fusion of the fragments. Intuitively, these findings can be understood in terms of the combined effect of the Coulomb barriers of the proton and ^{7}Be with the target A, and their proportional incident energies. That is, the relative incident energy of the proton and ^{7}Be are $E_{lab,p} = (\frac{1}{8})E_{lab}$ and

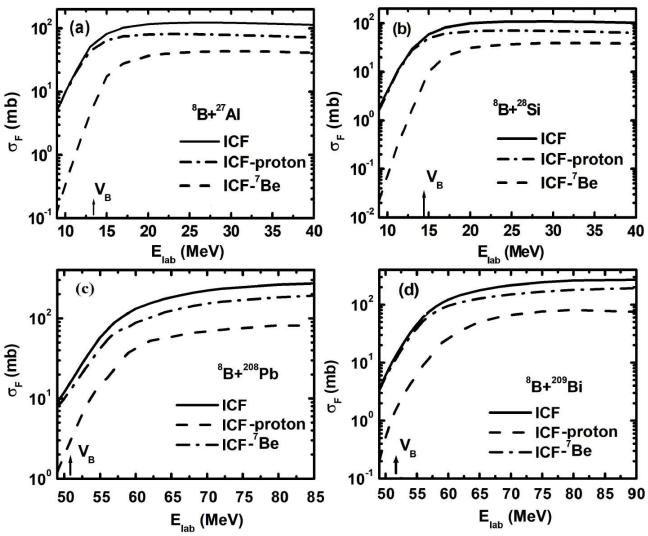

Figure 3. Incomplete fusion for ^{8}B and contributions from its fragments ^{7}Be and proton.

$E_{lab,^7Be} = (\frac{7}{8})E_{lab}$ respectively. In the center of mass of the fragments and the target with mass m_A, we have,

$$E_{cm,p-A} = (\frac{1}{8})\frac{m_A}{(m_A+1)}E_{lab}, \tag{23}$$

$$E_{cm,^7Be-A} = (\frac{7}{8})\frac{m_A}{(m_A+7)}E_{lab}. \tag{24}$$

Classically, fusion starts becoming easier for energies above the $l = 0$ barriers of the fragments with the target, $V_{B,p-A}$ and $V_{B,^7Be-A}$. That is, for energies E_{lab} that satisfy, $\Delta E_{cm,p-A} \geqslant 0$ and $\Delta E_{cm,^7Be-A} \geqslant 0$, where,

$$\Delta E_{cm,p-A} = E_{cm,p-A} - V_{B,p-A}, \tag{25}$$

$$\Delta E_{cm,^7Be-A} = E_{cm,^7Be-A} - V_{B,^7Be-A}, \tag{26}$$

or,

$$\Delta E_{cm,p-A} = (\frac{1}{8})\frac{m_A}{(m_A+1)}E_{lab} - V_{B,p-A}, \tag{27}$$

and,

$$\Delta E_{cm,^7Be-A} = (\frac{7}{8})\frac{m_A}{(m_A+7)}E_{lab} - V_{B,^7Be-A}. \tag{28}$$

Otherwise, the fragments have to penetrate their respective barriers. For instance, for the target ^{208}Pb, in the energy range $55 < E_{lab} < 85$ MeV. If $V_{p-^{208}Pb} \sim 10.56$ Mev and $V_{^7Be-^{208}Pb} \sim 39.38$ MeV, it is true that, $\Delta E_{cm,p-A} < 0$ and $\Delta E_{cm,^7Be-A} > 0$. Thus, fusion of ^{7}Be becomes easier than for proton in this energy range. For the target ^{209}Bi something similar happens. A similar explanation applies to the lighter ^{27}Al, but the situation depends strongly on E_{lab}. If $V_{B,p-^{27}Al} \sim 2.29$ MeV and $V_{B,^7Be-^{27}Al} \sim 8.34$ MeV, then for E_{lab} energies below 11 MeV, $\Delta E_{cm,p-^{27}Al}$ and $\Delta E_{cm,^7Be-^{27}Al}$ are both negative, but $|\Delta E_{cm,^7Be-^{27}AL}| > |\Delta E_{cm,p-^{27}Al}|$. In this case, quantum penetration of the barrier occurs for both fragments, but for ^7Be for

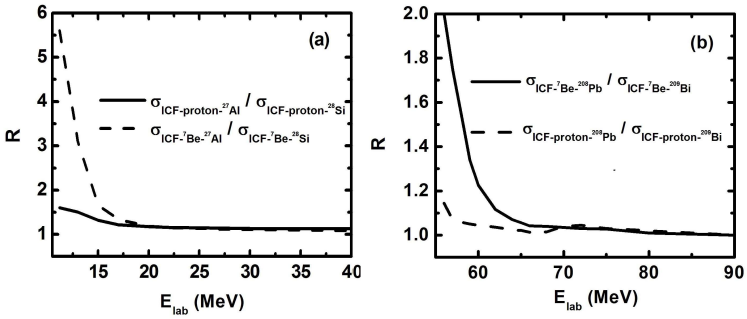

Figure 4. Ratio of incomplete fusion for proton and ^{7}Be for the targets ^{27}Al and ^{28}Si as well as for ^{208}Pb and ^{209}Bi.

energies $E_{cm,^{7}Be} < 11$ MeV, the barrier is wider. So, intuitively it may be concluded that the incomplete fusion of the proton dominates for energies below 11 MeV. For higher energies the situation inverts and the incomplete fusion of ^{7}Be begins to grow more rapidly. For the target ^{28}Si something similar happens.

Finally in Fig. (4a-4b), the ratio of incomplete fusion of the proton for ^{27}Al respect to ^{28}Si, as well as for ^{7}Be are presented. The same ratios for the targets ^{208}Pb and ^{209}Bi are also shown. These figures show that, as the energy decreases towards the barrier, the ICF suppression for both fragments of ^{28}Si and ^{209}Bi respect ^{27}Al and ^{208}Pb. That is, the additional proton of ^{28}Si and ^{209}Bi enhances the fragment-target barrier which in turn, produces the suppression. As observed, the suppression is larger for ^{7}Be than for the proton.

4 Summary

Calculations of total, complete and incomplete fusion cross sections for reactions of the weakly bound nucleus ^{8}B with targets ^{27}Al, ^{28}Si, ^{208}Pb and ^{209}B have been presented for energies around and above the Coulomb barrier. The calculations have been done in two steps. a) The radial wave function of the relative motion between the projectile ^{8}B with the targets have been determined from CDCC calculations. 2) These radial wave functions are in turn used to calculate the angular momentum probabilities of the different fusion mechanisms. The conclusions obtained from these calculations are:

1. For energies around and above the barrier, incomplete fusion becomes more important than complete fusion for the lighter nuclei, ^{27}Al, and ^{28}Si. For the heavier targets ^{208}Pb and ^{209}Bi, complete fusion is the most important component of total fusion.

2. Incomplete fusion from the breakup components of ^{8}B, proton and ^{7}Be, have been calculated and the specific contributions to the total incomplete fusion have been established for the different targets.

3. Proton incomplete fusion dominates over that of ^{7}Be for the lighter targets, however, for the heavy ^{208}Pb and ^{209}Bi, incomplete fusion due to ^{7}Be accounts for most of incomplete fusion.

4. Intuitively, the points mentioned above, can be understood in terms of : The mass and charge of the targets, specifically the *proton − target*, ^{7}*Be − target* Coulomb barriers, as well as, the relative incident fragment energies of the proton and ^{7}*Be*.

References

[1] L. F. Canto, P. R. S. Gomes, R. Donangelo, and M. S. Hussein, Phys. Rep. **424**, 1 (2006)
[2] J. F. Liang, C. Signorini, Int. J. Mod. Phys. E **14**, 1121 (2005)
[3] N. Keeley, R. Raabe, N. Alamanos, and J. L. Sida, Prog. Part. Nucl. Phys. **59**, 579 (2007)
[4] K. Hagino and N. Takigawa, Prog. Theor. Phys. **128**, 1061 (2012)
[5] B.B. Back, H. Esbensen, C. L. Jiang, and K. E. Rehm, Rev. Mod. Phys. **86**, 317 (2014)
[6] L. F. Canto, P. R. S. Gomes, R. Donangelo, J. Lubian, and M. S. Hussein, Phys. Rep. **596**, 1 (2015)
[7] F.A.Souza, C. Beck, N. Carlin, N. Keeley, R. Liguori Neto, M.M. de Moura, M.G. Munhoz, M.G. Del Santo, A.A.P. Suaide, E.M. Szanto A. Szanto de Toledo, Nucl. Phys. A **821**, 36 (2009)
[8] F.A. Souza, N. Carlin, C. Beck, N. Keeley, A. Diaz-Torres, R. Liguori Neto, C. Siqueira-Mello, M.M. de Moura, M.G. Munhoz, R.A.N. Oliveira, M.G. Del Santo, A.A.P. Suaide, E.M. Szanto, A. Szanto de Toledo, Eur. Phys. J. A **44**, 181 (2010)
[9] Jin Lei and Antonio M. Moro, Phys. Rev. Lett. **122**, 042503 (2019)
[10] K. Hagino, A. Vitturi, C.H. Dasso, S.M. Lenzi, Phys. Rev. C **61**, 037602 (2000)
[11] C. Beck, N. Rowley, P. Papka, S. Courtin, et el., Nucl. Phys. A **834**, 440c (2010)
[12] D. H. Luong et al., Phys. Lett. B **695**, 105 (2011)
[13] D. H. Luong, M. Dasgupta, D. J. Hinde, R. du Rietz, R. Rafiei, C. J. Lin, M. Evers, A.Diaz-Torres, Phys. Rev. C **88**, 034609 (2013)
[14] R. Rafiei, R. du Rietz, D. H. Luong, D. J. Hinde, M. Dasgupta, M. Evers, and A. Diaz-Torres, Phys. Rev. C **81**, 024601 (2010)
[15] A. Shrivastava et al., Phys. Lett. B **633**, 463 (2006)
[16] Y. Sakuragi, M. Yahiro, M. Kamimura, Prog. Theor. Phys. Suppl., **89**, 1 (1986)
[17] Y. Sakuragi, M. Yahiro, M. Kamimura, Prog. Theor. Phys. **70**, 1047 (1983)
[18] N. Austern, Y. Iseri, M. Kamimura, et al, Phys. Rep., **154**, 125 (1987)
[19] A. Diaz-Torres, I.J. Thompson, C. Beck, Phys. Rev. C, **68**, 044607 (2003)
[20] V.V. Parkar, V. Jha, S. Kailas, Phys. Rev. C, **94**, 024609 (2016)
[21] A. Diaz-Torres, D.J. Hinde, J.A. Tostevin, M. Dasgupta, L.R. Gasques, Phys. Rev. Lett., **98**, 152701 (2007)
[22] A. Diaz-Torres, J. Phys. G, Nucl. Part. Phys. **37**, 075109 (2010)
[23] A. Diaz-Torres, D. Quraishi, Phys. Rev. C **97**, 024611 (2018)
[24] J. Rangel, M.R. Cortes, J. Lubian, L.F. Canto, Phys. Lett B **803**, 135337 (2020)
[25] M.R. Cortes, J. Rangel, J.L. Ferreira, J. Lubia, L.F. Canto, Phys. Rev. C **102**, 064628 (2020)
[26] J. Lubian, J.L. Ferreira, J. Rangel, M.R. Cortes, L.F. Canto, Phys. Rev. C **105**, 054601 (2022)
[27] L.F. Canto, J. Rangel, J. Lubian, CF-ICF computer code (unpublished)
[28] I.J. Thompson, Comput. Phys. Rep., **7**, 167 (1988)
[29] G.R. Satchler, M.A. Nagarajan, J.S. Liley, I.J. Thompson, Ann. Phys. (NY) **178**, 110 (1987)
[30] G. Potel, F.M. Nunes, I.J. Thompson, Phys. Rev. C **92**, 034611 (2015)
[31] L.C. Chamon, D. Pereira, M.S. Hussein, M. A. Candido Ribeiro, D. Galetti, Phys. Rev. Lett. **79**, 5218 (1997)
[32] L.C. Chamon, B.V. Carlson, L.R. Gasques, D. Pereira, C. De Conti, M.A.G. Alvarez, M.S. Hussein, M.A. Candido Ribeiro, E.S. Rossi Jr., C.P. Silva, Phys. Rev. C **66**, 014610

(2002)

[33] J. Rangel, J. Lubian, L.F. Canto P.R.S. Gomes, Phys. Rev. C **93**, 054610 (2016)

[34] A. Pakou, E. Stiliaris, D. Pierroutsakou, N. Alamanos, A. Boiano, C. Boiano, D. Filipescu, T. Glodariu, J. Grebosz, A. Guglielmetti, M. La Commara, M. Mazzocco, C. Parascandolo, K. Rusek, A. M. Sánchez-Benítez, C. Signorini, O. Sgouros, F. Soramel, V. Soukeras, E. Strano, L. Stroe, N. Toniolo, D. Torresi, and K. Zerva Phys. Rev. C **87**, 014619, (2013).